JACS
JOURNAL OF THE AMERICAN CHEMICAL SOCIETY
Communication
pubs.acs.org/JACS

Fullerene Crystals with Bimodal Pore Architectures Consisting of Macropores and Mesopores

Lok Kumar Shrestha,*[,†,‡] Yusuke Yamauchi,*[,†,∥,⊥] Jonathan P. Hill,[†] Kun'ichi Miyazawa,[§] and Katsuhiko Ariga*[,†,∥]

[†]World Premier International Center for Materials Nanoarchitectonics (WPI-MANA), [‡]International Centre for Young Scientists (ICYS), and [§]Fullerene Engineering Group, National Institute for Materials Science (NIMS), 1-1 Namiki, Tsukuba 305-0044, Japan

[∥]PRESTO & CREST, JST, 1-1 Namiki, Tsukuba 305-0044, Japan

[⊥]Faculty of Science and Engineering, Waseda University, 3-4-1 Okubo, Shinjuku, Tokyo 169-8555, Japan

Supporting Information

ABSTRACT: A new class of fullerene (C_{60}) crystals with bimodal pore architectures consisting of macropores and mesopores was synthesized by using a liquid–liquid interfacial precipitation (LLIP) method involving an interface between isopropyl alcohol (IPA) and a saturated solution of C_{60} in a mixture of benzene and carbon tetrachloride (CCl_4). By varying the mixing fraction of CCl_4 in benzene, the porosity and electrochemically active surface area can be flexibly controlled.

Fullerene (C_{60}) is the most investigated molecule of the family of carbons due to its extensive potential applications in semiconductors and optoelectrical devices and also in biomedicals.[1] Its electron deficiency (i.e., it is an electron acceptor) has been widely utilized in combination with suitable electron donors for development of heterojunctions capable of generating a photocurrent.[2] Introduction of multiple pores in bulk C_{60} crystals can drastically increase the effective surface area, which is of great utility in many applications (e.g., high-power solar cells and capacitors, large hydrogen storages, highly active photocatalysts, highly sensitive chemical and physical sensors). Our target at the outset of this study was to realize new C_{60} crystals with porous structures.

Currently, development of novel synthetic approaches to nano/mesoporous materials with perfectly crystalline frameworks is a challenging issue. Surfactant-mediated synthetic strategies have been widely used to fabricate many nano/mesoporous materials of different compositions (e.g., transition-metal oxides, carbons, inorganic–organic hybrid materials, polymers, and metals).[3,4] The framework compositions strongly influence the properties of these nano/mesoporous materials. In almost all cases, however, the materials have amorphous frameworks that can limit their practical usage.

Until now, several efforts have been made to increase the crystallinity of the frameworks. In the case of nano/mesoporous metal oxides, controlled thermal and hydrothermal treatments have resulted in effective crystallization.[4] However, large structural variations, such as "pore expansion", can occur through fusion of several pores during framework crystallization, which seriously reduces the surface area.[4] Several groups have reported mesoporous organosilica containing perfectly crystallized frameworks,[5] and Inagaki et al. demonstrated its great utility as a light-harvesting material.[5f] Recently, Ryoo et al. synthesized mesoporous zeolites and demonstrated their high catalytic activity for various acid-catalyzed reactions involving bulky molecules.[6] Thus, by considering highly crystalline frameworks, we can discover novel solid-state properties or dramatically improve inherent properties in ways that cannot be realized in amorphous or poorly crystallized frameworks.[7]

Herein, we report a preparation of novel C_{60} crystals with bimodal pore architectures consisting of macropores and mesopores by interfacing a solution of a mixture of two different solvents with a particular antisolvent (Figure 1).

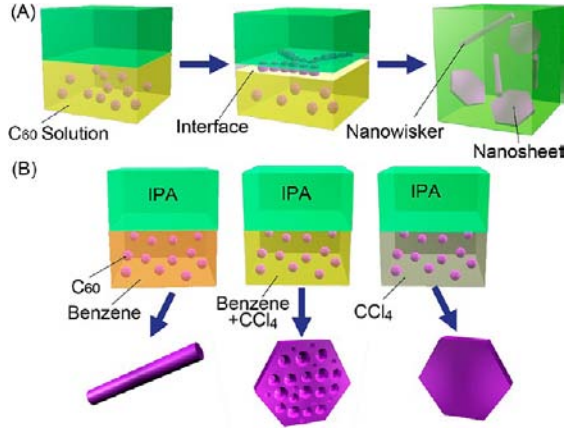

Figure 1. (A) Synthetic routes of C_{60} crystallization using a LLIP method. (B) Preparation of C_{60} crystals with various shapes.

Under the optimized condition, well-defined two-dimensional (2D) hexagonal sheet morphology was obtained, and the pore walls were highly crystallized. Our synthetic concept is based on a liquid–liquid interfacial precipitation (LLIP) method,[8] which is the most promising methodology to produce C_{60} crystals of controlled morphology. Although various methods have been developed for production of shape-controlled C_{60} crystals, the LLIP method is well-known, and various C_{60} crystal

Received: November 5, 2012
Published: December 31, 2012

dx.doi.org/10.1021/ja3108752 | J. Am. Chem. Soc. 2013, 135, 586–589

morphologies have been synthesized in binary solvent (a solvent and an antisolvent) systems where the morphology of C_{60} crystals can be freely controlled by selecting suitable solvents and antisolvents (e.g., poor solvents for C_{60} are alcohols), crystallization temperature, and volume ratios of solvents and antisolvents.[8c−f,9] However, C_{60} crystals with porous structures have not been previously reported. We believe that our concept of mixing solvents represents a novel method for preparation of new nanostructured C_{60} crystals with porous structures.

Prior to the synthesis of C_{60} crystals with porous structures, the following two systems had been studied: isopropyl alcohol (IPA)/benzene and IPA/carbon tetrachloride (CCl_4) systems (Figure 1). These systems respectively resulted in 1D and 2D morphologies without macro- and mesopores. For the synthesis of C_{60} crystals with porous structures, the synergistic effect of mixing solvents (CCl_4 and benzene) on the C_{60} crystal morphology with fixing of IPA amount as the antisolvent was studied. Saturated solutions of C_{60} were prepared in mixtures of CCl_4 and benzene at different mixing ratios (w/w): CCl_4:benzene = 30:70, 50:50, 70:30, 80:20, and 90:10. Concentrations of C_{60} in mixed CCl_4:benzene were found to be 1.16 mg·mL^{-1} (for CCl_4:benzene = 30:70), 0.98 mg·mL^{-1} (for CCl_4:benzene = 50:50), 0.76 mg·mL^{-1} (for CCl_4:benzene = 70:30), 0.65 mg·mL^{-1} (for CCl_4:benzene = 80:20), and 0.54 mg·mL^{-1} (for CCl_4:benzene = 90:10) at 25 °C. In a typical crystallization, IPA and C_{60} solutions were kept in a temperature-controlled water bath at 5 °C for 30 min prior to mixing. After mixing, solutions were sonicated for 5 min and kept in an incubator with temperature maintained at 5 °C for 24 h for the crystal growth. The detailed synthetic method is given in the Supporting Information (SI).

Figures 2 and S2 show typical SEM images of 2D hexagonal sheets synthesized at different mixing ratios of CCl_4 and benzene by the LLIP method. In the absence of CCl_4, i.e., in the IPA/benzene system, 1D nanowhiskers with average diameters of 100−300 nm and lengths of a few tens-to-hundreds of micrometers were obtained (Figure S2.1). However, a surprising morphological change from 1D nanowhiskers to 2D hexagonal sheets was observed upon incorporation of 30% CCl_4 in the system, i.e., in the CCl_4:benzene = 30:70 system (Figures 2a and S2.2). Miyazawa et al.[8a,c] have proposed a rolling up mechanism for the formation of 1D whiskers, i.e., 2D nanosheet rolls up and forms 1D rods. Here, we have observed the opposite structural transformation. This indicates that the presence of CCl_4 prevents the rolling up process and stabilizes the 2D sheet structure. The average size of these crystalline sheets was about 5 μm with thicknesses from 800 nm to 1 μm. C_{60} crystals with similar 2D sheet morphology were observed in the CCl_4:benzene = 50:50 system (Figures 2b and S2.3). In these systems, porous structures were not developed. However, when the mixing ratio of CCl_4 was further increased, a porous structure was generated on the surface of the hexagonal sheet (Figure 2c−f). For instance, macropores can clearly be seen on the surface of 2D hexagonal-shaped crystals prepared from the CCl_4:benzene = 70:30 system, and the average size of pores was found to be about 200 nm (see Figures 2c and S2.4). The number and size of the pores were increased with further increase in the proportion of CCl_4 (Figures 2d−f and S2.5 and S2.6). In the CCl_4:benzene = 90:10 system, the average pore size was found to be around 400 nm.

In order to investigate whether these macropores are present throughout the hexagonal sheet and/or if there is any mesoporous structure in the bulk of the 2D crystals, we measured cross sections of the materials by TEM (Figures 3 and S3). The samples for these observations were prepared by sectioning hexagonal sheet using focused ion beam (FIB). Cross-sectional TEM images of the C_{60} crystals obtained from the IPA/(CCl_4:benzene = 80:20) and IPA/(CCl_4:benzene = 90:10) systems were shown in Figures 3, S3.3, and S3.4. Cross-sectional TEM images unambiguously reveal a well-developed mesoporous structure in these systems. However, in the case of IPA/(CCl_4:benzene = 50:50 and 70:30) systems, the mesoporous structure was not fully developed, and only a

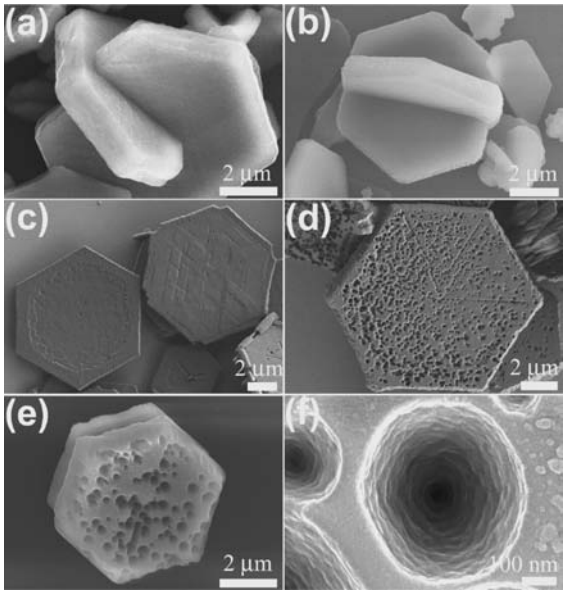

Figure 2. (a−e) SEM images of C_{60} crystals prepared in mixed systems of IPA/(CCl_4+benzene) at different mixing ratios of CCl_4. CCl_4:benzene = (a) 30:70, (b) 50:50, (c) 70:30, (d) 80:20, and (e) 90:10. (f) High-resolution SEM image of macropore on the surface of C_{60} crystal observed in system (e).

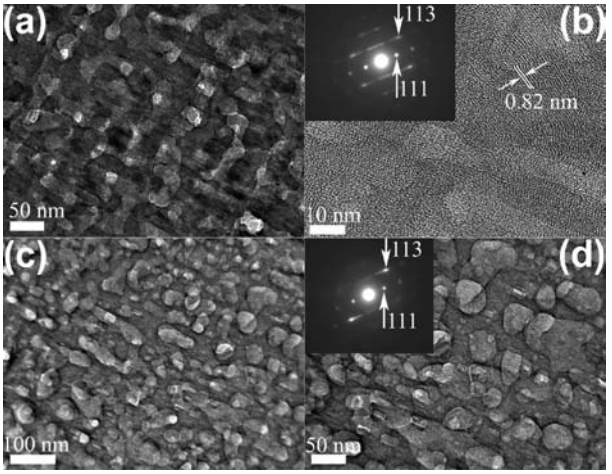

Figure 3. Cross-sectional TEM images and selected area ED patterns of C_{60} crystals with porous structures synthesized at two different mixing ratios of CCl_4 and benzene: (a,b) CCl_4:benzene = 80:20 and (c,d) CCl_4:benzene = 90:10.

dx.doi.org/10.1021/ja3108752 | J. Am. Chem. Soc. 2013, 135, 586−589

few mesopores could be observed in the crystals (Figures S3.1 and 3.2).

In the case of CCl_4:benzene = 80:20, the average pore size was in the range from 15 to 25 nm (Figure 4A). The mesopore

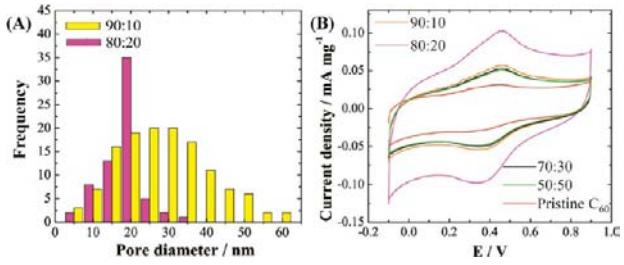

Figure 4. (A) Pore size distribution calculated from cross-sectional TEM images for C_{60} crystals obtained from the IPA/(CCl_4:benzene = 80:20 and 90:10) systems. (B) Cyclic voltammograms of C_{60} crystals obtained from IPA/(CCl_4:benzene = 50:50, 70:30, 80:20, and 90:10) systems. For comparison, the CV curve of pristine C_{60} is also included.

sizes and polydispersities appeared to increase with a gradual increase in mixing ratio of CCl_4 (Figures 3c,d and S3.4). Average pore size was found to be in the range from 20 to 40 nm for the CCl_4:benzene = 90:10 system (Figure 4A). The selected-area electron diffraction (ED) patterns shown in the inset of Figure 3b,d were indexed to 111 and 113 crystallographic planes of a face-centered cubic (*fcc*) crystalline structure of pristine C_{60}. Other ED patterns taken at different regions are given in Figure S4. As seen in high-magnification TEM images (Figures 3b and S3.5), lattice fringes coherently extend over several mesopores indicating that the pore walls were highly crystallized.

Nitrogen adsorption/desorption isotherms and the calculated total surface areas are given in the Figure S5. With increasing mixing ratios of CCl_4 above CCl_4:benzene >50:50, the total surface area increased up to 32.3 $m^2 \cdot g^{-1}$. The calculated surface area was relatively low in comparison with general porous carbon materials (Table S1), although cross-sectional TEM images showed a well-developed mesoporous structure. This highlights the fact that not all the mesopores present in the C_{60} crystals are accessible for nitrogen adsorption.

Careful observation of the porous structures at the surface of hexagonal sheets revealed the following features (Figure S2): (a) Pores mostly existed in the macroscale range (macropores) and were cone shapes; (b) height/depth of these cones increased with mixing ratio of CCl_4; and (c) the macropores were merged, leading to formation of giant pores at higher mixing ratios of CCl_4. From these observations, the C_{60} crystals with tunable numbers of pores and pore sizes can be synthesized simply by changing the mixing ratio of the two solvents.

To estimate the accessible surface areas, we performed electrochemical measurements on the obtained C_{60} crystals and the result is presented in Figure 4B. The experimental tests were carried out using cyclic voltammetry (CV) in 0.5 M H_2SO_4 in a potential range from −0.1 to 0.9 V (vs Ag/AgCl) at a scan rate of 5 $mV \cdot s^{-1}$. The CV curves are characteristic of carbon an electrical double-layer capacitor. The gravimetric specific capacitance increased with increase in the mixing ratio of CCl_4 in the system (Table S2). Thus, introduction of pores in C_{60} crystals caused the current density to increase in comparison with pristine C_{60} crystals without pores. Our data show that the C_{60} crystals prepared from the CCl_4:benzene = 80:20 system exhibited the highest current density, providing a larger electrochemically active surface area.

Powder X-ray diffraction (XRD) patterns and Raman spectra of the synthesized C_{60} crystals are shown in Figure 5A,B,

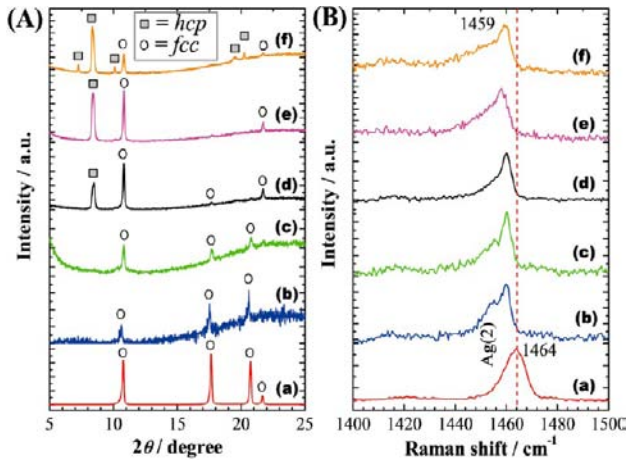

Figure 5. (A) XRD patterns and (B) Raman spectra for C_{60} crystals obtained under the IPA/(CCl_4:benzene) systems at different mixing ratio of CCl_4: (a) pristine C_{60}, (b) CCl_4:benzene = 30:70, (c) 50:50, (d) 70:30, (e) 80:20, and (f) 90:10.

respectively. XRD patterns of samples up to CCl_4:benzene = 50:50 were indexed as a *fcc* crystalline structure of pristine C_{60}. The lattice parameters of *fcc* crystal were a = 1.43 and 1.42 nm for CCl_4:benzene = 30:70 and 50:50, respectively. On the other hand, XRD patterns of samples at higher mixing ratios of CCl_4 can be assigned as mixed crystalline structures containing *fcc* (a = 1.42, 1.40, and 1.39 nm for CCl_4:benzene = 70:30, 80:20, and 90:10, respectively) and hexagonal closed packed (*hcp*) crystalline structures (a, c = 2.29, 1.40 nm; a, c = 2.29, 1.16 nm; and a, c = 2.00, 1.41 nm for CCl_4:benzene = 70:30, 80:20, and 90:10, respectively). The *hcp* crystalline C_{60} structure has often been observed in C_{60} nano- and microcrystals prepared by LLIP methods due to entrapment of solvent molecules.[10] Similar structures have been reported by Skokan et al. for crystals obtained by evaporation of a C_{60} solution in an organic solvent.[11] We note that the mixed *fcc* and *hcp* structures were only obtained in samples that exhibited a porous structure. We believe that slow evaporation of the entrapped solvent molecules may account for the formation of a porous structure. Raman spectra of samples show a significant shift toward lower frequency of the Ag(2) band peak to 1459 cm^{-1} compared to pristine C_{60} in which the Ag(2) band peak appears at 1464 cm^{-1}, corresponding to the pentagonal pinch mode. This frequency shift can be attributed to polymerization possibly occurring during Raman scattering measurements due to laser irradiation. Similar photopolymerization has been reported in C_{60} nanowhiskers.[8d,e]

In summary, we have prepared a new class of nanostructured carbon material, C_{60} crystals with bimodal pore architectures consisting of macropores and mesopores, following a new synthetic concept in C_{60} bottom-up nanotechnology. The obtained C_{60} crystals with bimodal pore architectures showed 2D hexagonal plate-like morphology and offered enhanced electrochemically active surface areas compared to pristine C_{60}. We are currently designing photovoltaic devices using our materials in combination with suitable electron-donor mole-

dx.doi.org/10.1021/ja3108752 | J. Am. Chem. Soc. 2013, 135, 586−589

cules, such as porphyrin or pentacene, and we will study their efficiency for the generation of photocurrent. In this study, we undertook electrochemical CV tests as a preliminary trial of materials' properties. Real applications will be the next issue for this project. We believe that our C_{60} material might be of great use in the fabrication of nanodevices (including organic solar cells and miniaturized organic superconductors) based on the unique concept of materials nanoarchitectonics.

■ ASSOCIATED CONTENT

Supporting Information

Detailed experimental procedures, additional SEM and TEM images, selected-area ED patterns, nitrogen adsorption/desorption isotherms, total surface areas, and preliminary electrochemical data. This material is available free of charge via the Internet at http://pubs.acs.org.

■ AUTHOR INFORMATION

Corresponding Author

shrestha.lokkumar@nims.go.jp; yamauchi.yusuke@nims.go.jp; ariga.katsuhiko@nims.go.jp

Notes

The authors declare no competing financial interest.

■ ACKNOWLEDGMENTS

L.K.S. thanks International Center for Materials Nanoarchitectonics (WPI-MANA) and National Institute for Materials Science (NIMS) for financial support. Technical assistance of Dr. Qingmin Ji at International Center for Materials Nanoarchitectonics (WPI-MANA) and National Institute for Materials Science (NIMS) is highly acknowledged.

■ REFERENCES

(1) (a) Haddon, R. C.; Brus, L. E.; Raghavachari, K. *Chem. Phys. Lett.* **1986**, *125*, 459−464. (b) Komatsu, K.; Murata, M.; Murata, Y. *Science* **2005**, *307*, 238−240. (c) Xing, Y. J.; Jing, G. Y.; Xu, J.; Yu, D. P. *Appl. Phys. Lett.* **2005**, *87*, 263117−263119. (d) Shin, H. S.; Yoon, S. M.; Tang, Q.; Chon, B.; Joo, T.; Choi, H. G. *Angew. Chem., Int. Ed.* **2008**, *47*, 693−696. (e) Zhou, S.; Burger, C.; Chu, B.; Sawamuraa, M.; Nagahama, N.; Toganoh, M.; Hackler, U. E.; Isobe, H.; Nakamura, E. *Science* **2001**, *291*, 1944−1947. (f) Homma, T.; Harano, K.; Isobe, H.; Nakamura, E. *Angew. Chem., Int. Ed.* **2010**, *49*, 1665−1668.

(2) (a) Sariciftci, N. S.; Smilowitz, L.; Heeger, A. J.; Wudl, F. *Science* **1992**, *258*, 1474−1476. (b) Chu, C. W.; Shao, Y.; Shrotriya, V.; Yang, Y. *Appl. Phys. Lett.* **2005**, *86*, 243506−3. (c) Huang, J.; Yang, Y. *Appl. Phys. Lett.* **2007**, *91*, 203505−3. (d) Oku, T.; Kakuta, N.; Kawashima, A.; Nomura, K.; Motoyoshi, R.; Suzuki, A.; Kikuchi, K.; Kinoshita, G. *Mater. Trans.* **2008**, *49*, 2457−2460. (e) Lee, J. K.; Ma, W. L.; Brabec, C. J.; Yuen, J.; Moon, J. S.; Kim, J. Y.; Lee, K.; Bazan, G. C.; Heeger, A. J. *J. Am. Chem. Soc.* **2008**, *130*, 3619−3623. (f) Chellappan, V.; Ng, G. M.; Tan, M. J.; Goh, W. P.; Zhu, F. *Appl. Phys. Lett.* **2009**, *95*, 263305−3. (g) Matsuo, Y.; Sato, Y.; Niinomi, T.; Soga, I.; Tanaka, H.; Nakamura, E. *J. Am. Chem. Soc.* **2009**, *131*, 16048−16050. (h) Xiao, Z.; Matsuo, Y.; Soga, I.; Nakamura, E. *Chem. Mater.* **2012**, *24*, 2572−2582.

(3) (a) Ariga, K.; Vinu, A.; Yamauchi, Y.; Qingmin, J.; Hill, J. P. *Bull. Chem. Soc. Jpn.* **2012**, *85*, 1−32. (b) Wan, Y.; Zhao, D. *Chem. Rev.* **2007**, *107*, 2821−2860.

(4) (a) Lee, B.; Lu, D.; Kondo, J. N.; Domen, K. *Chem. Commun.* **2001**, 2118−2119. (b) Urade, V. N.; Hillhouse, H. W. *J. Phys. Chem. B* **2005**, *109*, 10538−10541.

(5) (a) Inagaki, S.; Guan, S.; Ohsuna, T.; Terasaki, O. *Nature* **2002**, *416*, 304−307. (b) Kapoor, M. P.; Yang, Q.; Inagaki, S. *J. Am. Chem. Soc.* **2002**, *124*, 15176−15177. (c) Lerouge, F.; Cerveau, G.; Corriu, R. J. P. *New J. Chem.* **2006**, *30*, 1364−1376. (d) Hoffmann, F.; Cornelius, M.; Morell, J.; Froba, M. *Angew. Chem., Int. Ed.* **2006**, *45*, 3216−3251. (e) Fujita, S.; Inagaki, S. *Chem. Mater.* **2008**, *20*, 891−908. (f) Inagaki, S.; Ohtani, O.; Goto, Y.; Okamoto, K.; Ikai, M.; Yamanaka, K.; Tani, T.; Okada, T. *Angew. Chem., Int. Ed.* **2009**, *48*, 4042−4046.

(6) (a) Na, K.; Choi, M.; Ryoo, R. *Microporous Mesoporous Mater.* **2012**, *166*, 3−19. (b) Na, K.; Jo, C.; Kim, J.; Cho, K.; Jung, J.; Seo, Y.; Messinger, R. J.; Chmelka, B. F.; Ryoo, R. *Science* **2011**, *333*, 328−332.

(7) (a) Mizoshita, N.; Ikai, M.; Tani, T.; Inagaki, S. *J. Am. Chem. Soc.* **2009**, *131*, 14225−14227. (b) Waki, M.; Mizoshita, N.; Tani, T.; Inagaki, S. *Angew. Chem., Int. Ed.* **2011**, *50*, 11667−11671. (c) Mizoshita, N.; Tani, T.; Shinokubo, H.; Inagaki, S. *Angew. Chem., Int. Ed.* **2012**, *51*, 1156−1160.

(8) (a) Miyazawa, K.; Kuwasaki, Y.; Obayashi, A.; Kuwabara, M. *J. Mater. Res.* **2002**, *17*, 83−88. (b) Xu, M.; Pathak, Y.; Fujita, D.; Ringor, C.; Miyazawa, K. *Nanotechnology* **2008**, *19*, 075712. (c) Sathish, M.; Miyazawa, K.; Sasaki, T. *Chem. Mater.* **2007**, *19*, 2398−2400. (d) Sathish, M.; Miyazawa, K. *J. Am. Chem. Soc.* **2007**, *129*, 13816−13817. (e) Sathish, M.; Miyazawa, K.; Hill, J. P.; Ariga, K. *J. Am. Chem. Soc.* **2009**, *131*, 6372−6373. (f) Jeong, J.; Kim, W. S.; Park, S. I.; Yoon, T. S.; Chung, B. H. *J. Phys. Chem. C* **2010**, *114*, 12976−12981.

(9) (a) Zheng, L.; Han, Y. *J. Phys. Chem. B* **2012**, *116*, 1598−1604. (b) Miyazawa, K.; Hotta, K. *J. Cryst. Growth* **2010**, *312*, 2764−2770. (c) Masuhara, A.; Tan, Z.; Kasai, H.; Nakanishi, H.; Oikawa, H. *Jpn. J. Appl. Phys.* **2009**, *48*, 050206−1−050206−3.

(10) (a) Ramm, M.; Luger, P.; Zobel, D.; Duczek, W.; Boeyens, J. C. A. *Cryst. Res. Technol.* **1996**, *31*, 43−53. (b) Collins, C.; Foulkes, J.; Bond, A. D.; Klinowski, J. *Phys. Chem. Chem. Phys.* **1999**, *1*, 5323−5326. (c) Korobov, M. V.; Stukalin, E. B.; Mirakyan, A. L.; Neretin, I. S.; Slovokho-tov, Y. L.; Dzyabchenko, A. V.; Ancharov, A. I.; Tolochko, B. P. *Carbon* **2003**, *41*, 2743−2755. (d) Miyazawa, K.; Nishimura, C.; Fujino, M.; Suga, T.; Yoshii, T. *Trans. Mater. Res. Soc. Jpn.* **2004**, *29*, 1965−1968. (e) Minato, J.; Miyazawa, K. *Carbon* **2005**, *43*, 2837−2841.

(11) (a) Skokan, E. V.; Privalov, V. I.; Arkhangelskii, I. V.; Davydov, V. Y.; Tamm, N. B. *J. Phys. Chem. B* **1999**, *103*, 2050−2053. (b) Skokan, E. V.; Arkhangelskii, I. V.; Zhukova, N. A.; Velikodnyi, Y. A.; Tamm, N. B.; Chelovskaya, N. V. *Carbon* **2003**, *41*, 1387−1389. (c) Skokan, E. V.; Arkhangelskii, I. V.; Izotov, D. E.; Chelovskaya, N. V.; Nikulin, M. M.; Velikodnyi, Y. A. *Carbon* **2005**, *43*, 803−808.